


ORIGINAL RESEARCH

Open Access



# Biochar-supported nano-scale zerovalent iron activated persulfate for remediation of aromatic hydrocarbon-contaminated soil: an in-situ pilot-scale study

Yu Zeng<sup>1,2</sup>, Tai Li<sup>1,3</sup>, Yingzhi Ding<sup>1,2</sup>, Guodong Fang<sup>1,2\*</sup> , Xiaolei Wang<sup>1,6</sup>, Bo Ye<sup>1,4</sup>, Liqiang Ge<sup>5</sup>, Juan Gao<sup>1,2</sup>, Yujun Wang<sup>1,2</sup> and Dongmei Zhou<sup>6</sup>

## Abstract

Biochar supported nano-scale zerovalent iron (nZVI/BC) for persulfate (PS) activation has been studied extensively for the degradation of pollutants on the lab scale, but it was rarely applied in practical soil remediation in the field. In this research, we developed a facile ball-milling method for the mass production of nZVI/BC, which was successfully applied to activate persulfate for the remediation of organic polluted soil on an in-situ pilot scale. In-situ high-pressure injection device was developed to inject nZVI/BC suspension and PS solution into the soil with a depth of 0–70 cm. The removal efficiency of target pollutants such as 2-ethylnitrobenzene (ENB, 1.47–1.56 mg/kg), biphenyl (BP, 0.19–0.21 mg/kg), 4-(methylsulfonyl) toluene (MST, 0.32–0.43 mg/kg), and 4-phenylphenol (PP, 1.70–2.46 mg/kg) at different soil depths was 99.7%, 99.1%, 99.9% and 99.7%, respectively, after 360 days of remediation. The application of nZVI/BC significantly increased the degradation rates of contaminants by 11–322%, ascribed to its relatively higher efficiency of free radical generation than that of control groups. In addition, it was found that nZVI/BC-PS inhibited soil urease and sucrase enzyme activities by 1–61% within 55 days due to the oxidative stress for microbes induced by free radicals, while these inhibition effects disappeared with remediation time prolonged (> 127 days). Our research provides a useful implementation case of remediation with nZVI/BC-PS activation and verifies its feasibility in practical contaminated soil remediation.

## Highlights

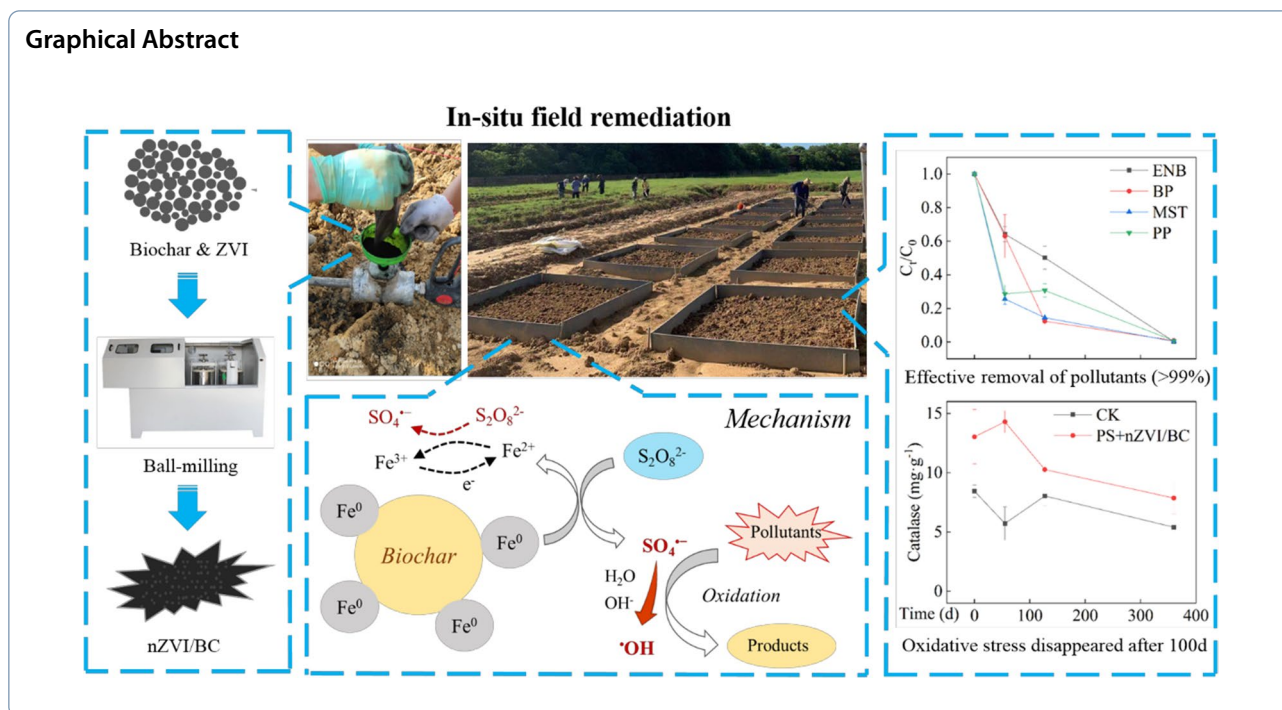
Biochar-supported nZVI for persulfate activation was applied in an in-situ pilot-scale remediation, which effectively removed pollutants by 99% with limited ecological risks.

**Keywords:** Persulfate, Biochar, Nanoscale zerovalent iron, Pilot-scale, Enzyme activities

\*Correspondence: [gdfang@issas.ac.cn](mailto:gdfang@issas.ac.cn)

<sup>1</sup> Key Laboratory of Soil Environment and Pollution Remediation, Institute of Soil Science, Chinese Academy of Sciences, Nanjing 210008, People's Republic of China

Full list of author information is available at the end of the article

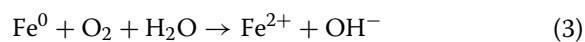
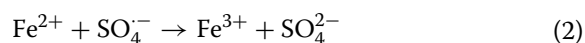
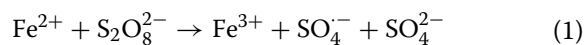


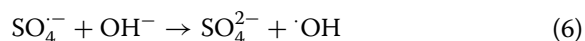
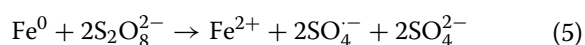
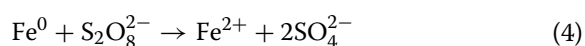
## 1 Introduction

The soil of industrial plants and their surrounding fields frequently suffer from organic pollution, posing a severe threat to humans, animals, and plants (Qiu et al. 2022). It is urgent to develop efficient, low-cost and environmentally friendly technologies for soil remediation in contaminated sites. Advanced oxidation processes (AOPs) have attracted increasing attention in remediation of soil and groundwater in recent years, due to their great potential to remove recalcitrant organic contaminants at a rapid speed to meet the usage of land in China (Wu et al. 2019a).

AOPs started with the Fenton reagent (hydrogen peroxide (H<sub>2</sub>O<sub>2</sub>) and Fe<sup>2+</sup>) on the basis of hydroxyl radicals (OH), which have a strong oxidation capacity to rapidly degrade different contaminants (e.g., pesticides, herbicides, and dyes) with second-reaction rate constants of  $\sim 10^8$ – $10^9$  M<sup>-1</sup> s<sup>-1</sup> in aqueous solutions (Dionysiou et al. 2000; Pignatello et al. 2006). However, H<sub>2</sub>O<sub>2</sub> is quickly consumed in the soil subsurface environment, which results in poor mobility and utilization efficiency of H<sub>2</sub>O<sub>2</sub> in soil remediation. Consequently, AOPs based on persulfate (PS) are an altered choice and have received increasingly interest in recent years (Delgado et al. 2020). PS is more stable than H<sub>2</sub>O<sub>2</sub>, which leads to PS having strong mobility and persisting in soil for more than 5 months (Yao et al. 2022). In addition, the sulfate radical (SO<sub>4</sub><sup>•-</sup>) generated from PS activation has comparable reactivity with OH, and can degrade a wide range of pollutants with more selectivity (Wu et al. 2021).

Zero-valent iron (ZVI) or nano-scale ZVI (nZVI) has been commonly employed for efficient activation of PS (Wang et al. 2008; Yao et al. 2014). PS is activated by ZVI to generate SO<sub>4</sub><sup>•-</sup>, and further produce OH by abstraction of electron from OH<sup>-</sup> or H<sub>2</sub>O (Eqs. 4–6) (Hazime et al. 2014). The application of ZVI can not only overcome the consumption of SO<sub>4</sub><sup>•-</sup> by excessive Fe<sup>2+</sup>, but also avoid introducing the quenchers such as anions (e.g., Cl<sup>-</sup> and SO<sub>4</sub><sup>2-</sup>), which would significantly improve the utilization efficiency of oxidant and the degradation efficiency of pollutants (Zhu et al. 2016). It has been reported that the application of nZVI for PS activation shows high efficiency in removing contaminants in aqueous solutions (Dong et al. 2017; Wu et al. 2018). However, applying nZVI in soil remediation encounters many challenges, including high aggregation tendency, easy oxidation, and high cost (Lu et al. 2020). It has been reported that dispersion of nZVI on supporting materials such as carbon materials, montmorillonite, and clay minerals is an effective method to overcome these drawbacks (Sun et al. 2021).





Biochar (BC) is an excellent supporting material with high porous structures and surface areas, which has been frequently used as a soil amendment and loading of catalysts in recent years (Zeng et al. 2022). It has been well demonstrated that biochar protects nZVI from agglomeration and rapid oxidation, and thus enhances the degradation of pollutants by PS activation with biochar supported nZVI (Shaheen et al. 2022). The degradation of organic contaminants in soil by persulfate activated with biochar-based materials has been widely studied on laboratory scales (Liu et al. 2022), but rarely investigated in field applications. For example, Yan et al. reported that the degradation efficiency of trichloroethylene by PS activated with biochar supported nZVI (nZVI/BC) increased by 75.6% compared with that of PS without biochar supporting (Yan et al. 2015). Guo et al. (2020) found that biochar derived from corn straw can effectively activate PS to degrade benzo(a) pyrene in soil. The application of nZVI/BC-PS for the degradation of bisphenol A in soil could also alleviate soil acidification during the PS decomposition process (Liu et al. 2020). The combination of nZVI/BC and PS was also used for decabromodiphenyl degradation in e-waste polluted soil (Li et al. 2019). The conventional metal-supported biochar material production methods contain pyrolysis, coprecipitation and hydrothermal carbonization (Yang et al. 2022). Unfortunately, these production methods are usually expensive and difficult to use in field applications due to the relative low yield of material production (Wu et al. 2020). In addition, the high cost to prepare nanomaterials is another limitation to the application of nZVI/BC in field. The knowledge on remediation of contaminated soil by nZVI/BC in field is rather limited. Consequently, an inexpensive, convenient and mass production method is needed to produce nZVI/BC for field remediation.

Therefore, the main objectives of this study were (1) to develop a balling method to batch synthesize nZVI/BC for field remediation; (2) to test the performance of nZVI/BC for PS activation and remediation of contaminated soil; (3) to evaluate its effect on soil properties such as enzyme activity. We chose an organic contaminated site in Yingtan, Jiangxi province (28.33° N, 117.21° E) to carry out an *in-situ* pilot-scale experiment. The preliminary investigation found that the soil of the contaminated site mainly contained 2-ethylnitrobenzene (ENB),

biphenyl (BP), 4-(methylsulfonyl) toluene (MST), and 4-phenylphenol (PP).

## 2 Materials and methods

### 2.1 Chemicals and materials

All chemicals used are listed in Additional file 1: Text S1. A planetary ball mill (XQM-60L) was used to prepare nZVI/BC modified from our previous study (Huang et al. 2021). Briefly, 4.0 kg iron powder was utterly mixed with 3.0 kg biochar powder in each mill pot, and then 22.5 kg stainless steel balls were added. The milling parameters were set as follows: rotation speed 120 r/min; forward rotation for 5 min and stop for 2 min; reverse rotation for 5 min and stop for 2 min; total running time 24, 48, 72, 96, and 120 h, respectively. The obtained solids were screened to separate nZVI/BC particles from steel balls. The mass production of nZVI/BC from these processes could reach up to 24 kg per day.

### 2.2 Contaminated site characterizations

The test site was located at Guixi, Yingtan City, Jiangxi Province (28.33° N, 117.21° E), near a pesticide chemical factory that mainly produced methyl sulfonate, *m*-hydroxybenzoic acid, and hydroxybiphenyl. The soil of this site was contaminated with 2-ethylnitrobenzene (ENB), biphenyl (BP), 4-(methylsulfonyl) toluene (MST), and 4-phenylphenol (PP) with corresponding concentrations of 1.47–1.56, 0.02–0.21, 0.32–0.43 and 1.7–2.46 mg/kg, respectively (Table 1). The depth of contaminant distribution ranged from 0 to 80 cm. The total remediation area of this project was ~82,600 m<sup>2</sup>, in which a test site with a dimension of ~22 m (length) × 7 m (width) × 1 m (depth) was reserved for our *in-situ* pilot-scale remediation research.

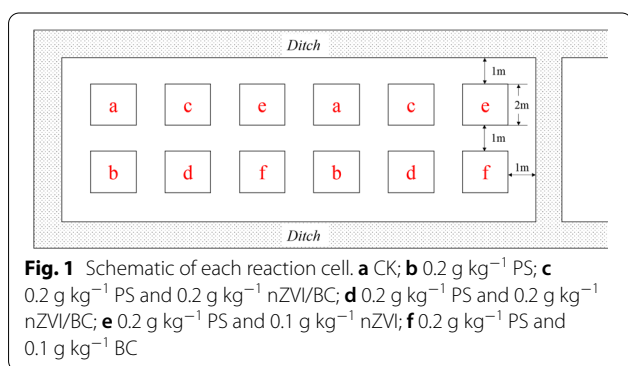
### 2.3 Injection of materials and oxidants

A total of 14 cells were designed (each cell was 2 × 2 m<sup>2</sup> and the interval between adjacent cells was 1 m), with 7 treatments and 2 replicates per treatment. The layout of the cells is shown in Fig. 1. To make nZVI/BC nanoparticles well dispersed in the heterogeneous soil system, we designed an *in-situ* high-pressure injection device to inject nanoparticle suspensions into soil. The device consists of a drug dispensing system, a high pressurizing system, a material feeding system and an injection gun head (Additional file 1: Fig. S1). High-pressure water was used to drive the nanomaterials to spray into the soil through the injection gun head, making the nanomaterials diffuse as evenly as possible into the soil. The hydraulic pressure was 10–300 MPa. The depth and radius of injection could reach 1 m and 2 m, respectively. Other related technical parameters are listed in Additional file 1: Table S1.

**Table 1** The concentrations of contaminants in soil before and after remediation with nZVI/BC (0.2 g kg<sup>-1</sup>) and PS (0.2 g kg<sup>-1</sup>)

Contaminant	Depth (cm)	Concentrations of contaminants (mg kg <sup>-1</sup> )			
		Original values	nZVI/BC 55 days	nZVI/BC 127 days	nZVI/BC 360 days
ENB	0–20	1.564 ± 0.251	1.004 ± 0.109	0.785 ± 0.212	0.004 ± 0.002
	20–40	1.470 ± 0.305	0.281 ± 0.276	0.231 ± 0.125	0.002 ± 0.001
	40–80	1.470 ± 0.305	1.243 ± 0.047	0.252 ± 0.029	0.167 ± 0.106
BP	0–20	0.191 ± 0.040	0.121 ± 0.039	0.024 ± 0.004	0.002 ± 0.000
	20–40	0.017 ± 0.003	0.002 ± 0.000	0.003 ± 0.001	0.001 ± 0.000
	40–80	0.207 ± 0.025	0.033 ± 0.006	0.021 ± 0.008	0.003 ± 0.001
MST	0–20	0.315 ± 0.015	0.081 ± 0.039	0.046 ± 0.007	ND
	20–40	0.415 ± 0.062	0.057 ± 0.032	0.026 ± 0.008	0.002 ± 0.000
	40–80	0.433 ± 0.097	0.184 ± 0.057	0.026 ± 0.008	0.003 ± 0.001
PP	0–20	1.702 ± 0.168	0.139 ± 0.042	0.128 ± 0.039	0.004 ± 0.002
	20–40	2.384 ± 0.287	0.175 ± 0.017	0.121 ± 0.011	0.011 ± 0.005
	40–80	2.460 ± 0.493	0.505 ± 0.076	0.210 ± 0.034	0.011 ± 0.005

ENB: 2-EthylNitrobenzene; BP: Biphenyl; MST: 4-(Methylsulfonyl) toluene; PP: 4-Phenylphenol



The dosage of nZVI/BC and concentration of persulfate used resulted from the preliminary experiments (Fig. 1). To make materials and oxidants well dispersed in heterogeneous soil system, the 2 × 2 m<sup>2</sup> plot was bisected into four 1 × 1 m<sup>2</sup> areas. The center points of these four areas and the center points of the plot were used as the injection points of materials. The injection depths were 10, 30, 50, and 70 cm in each injection point.

## 2.4 Analytical methods

### 2.4.1 nZVI/BC characterization

The hydration particle diameter of nZVI/BC was determined using a laser particle size analyzer (DLS, Malvern, UK). The composition of different samples was investigated using an X-ray diffraction powder diffractometer (XRD, Bruker, Germany). The surface morphology and structure of each sample were measured with a scanning electron microscope (SEM, FEI, USA). The particle

size distribution of the materials was analyzed by transmission electron microscope (TEM, FEI, USA).

### 2.4.2 Analysis of pollutants in contaminated soil

The types and concentrations of pollutants in soil were extracted with acetone and hexane, and then analyzed by gas chromatography-mass spectrometry (GC-MS, QP2020, Shimadzu, Japan). Briefly, 2.0 g soil was mixed with 5 mL acetone and 5 mL n-hexane, and shaken for 5 min, and then sonicated for 60 min. Finally, the supernatant was filtered by 0.22 μm membrane in a 50 mL long tail flask and evaporated, and hexane:dichloromethane (1:1) solution was added in constant with volume to 1 mL. Anhydrous sodium sulfate was used to dehydrate the sample. The recovery efficiency of pollutants ranged from 85% to 105% with these extraction procedures.

The sample was filtered through a 0.22 μm membrane for detection with a GC-MS. Chromatographic conditions were as follows: the initial temperature of the cylinder was 60 °C, the ion source temperature was 200 °C, the inlet temperature was 250 °C, the interface temperature was 250 °C, the pressure was 57.4 kPa, the total flow rate is 50.0 mL min<sup>-1</sup>, the column flow rate was 1.0 mL min<sup>-1</sup>, the linear velocity was 36.5 cm s<sup>-1</sup>, and the sampling was not separated. The heating procedure was 60 °C for 1 min, 10 °C min<sup>-1</sup> for 310 °C for 5 min, and the total running time was 31 min. The kinetics of target pollutant degradation were described with pseudo-first-order equation  $\ln(C_t/C_0) = -k_{\text{obs}} t$ , where the observed pseudo-first-order constants ( $k_{\text{obs}}$ ) of pollutant degradation were calculated. The soil enzyme activities including soil catalase, urease and sucrose

before and after remediation by nZVI/BC-PS were determined. The detailed analysis procedure is presented in Additional file 1: Text S2.

### 3 Results and discussion

#### 3.1 Characterizations of nZVI/BC

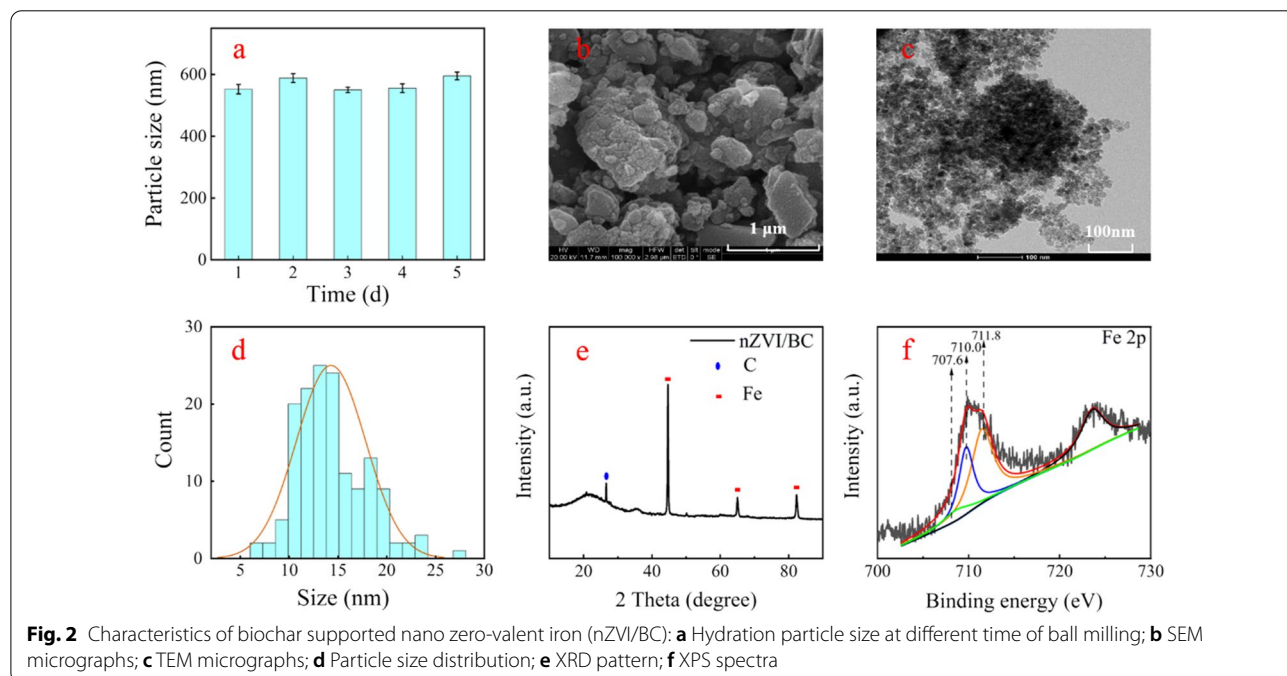
The hydrated particle size of nZVI/BC as a function of ball milling time is shown in Fig. 2a. The hydrated particle size of nZVI/BC particles reached 550 nm after one day of ball milling, and the change of particle size was insignificant with the extension of ball milling time. Considering the cost, one day is the optimized milling time, and SEM image shows that nZVI/BC surface is a clear nanosheet structure with spherical particles of finer particle size attached (Fig. 2b). The TEM image allows a clear view of the dark-colored nZVI/BC nanoparticles distributed on the carbon substrate with uniform size of 5–25 nm with an average particle size of 14.3 nm (Fig. 2c and d).

The XRD analysis of nZVI/BC shows that the broad reflection peaks at  $24.5^\circ$  belong to the amorphous graphitic structure (Fig. 2e) (Ouyang et al. 2017). The three diffraction peaks of  $2\theta$  at  $44.7^\circ$ ,  $65.0^\circ$  and  $82.4^\circ$  can be indexed to (110), (200) and (211) planes of nZVI. Apart from these, no other characteristic peaks were observed in the XRD patterns. As shown in Fig. 2f, XPS analysis of nZVI/BC shows that the Fe 2p peaks at 707.6 eV, 710.0 eV and 711.8 eV were attributed to Fe(0), Fe(II) and Fe(III), respectively (Wu et al. 2019b). The calculated Fe content on nZVI/BC particle surface was

10.66% for Fe(0), 33.78% for Fe(II) and 55.56% for Fe(III), respectively. These combined characterizations suggest that the BC was successfully loaded with nZVI on the carbon substrate and formed a stable crystalline structure with uniform particle size.

#### 3.2 Kinetics of pollutant degradation in soil

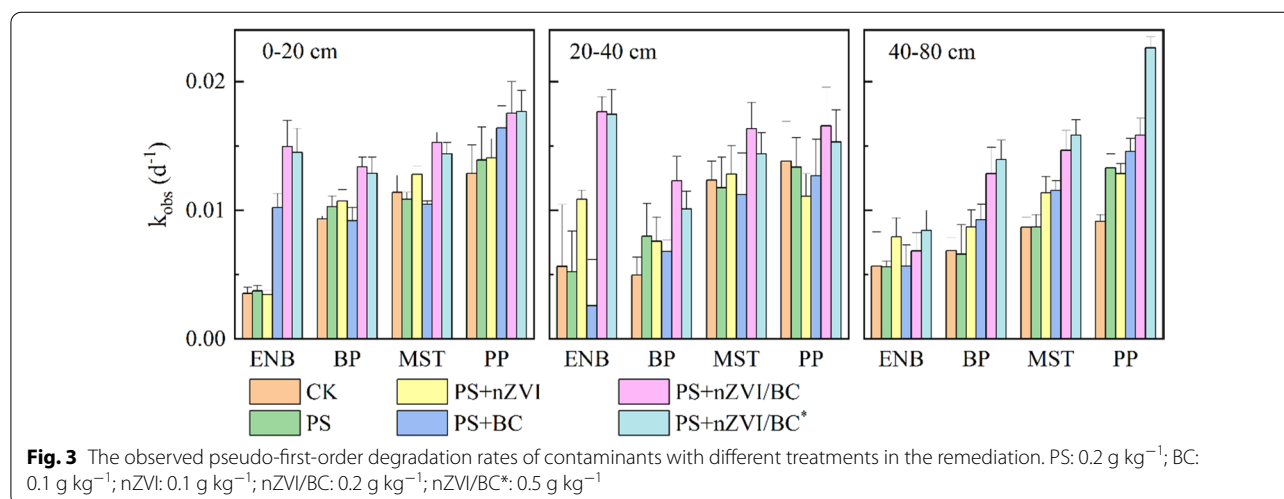
A combination of nZVI/BC ( $0.2 \text{ g kg}^{-1}$ ) and PS ( $0.2 \text{ g kg}^{-1}$ ) was injected to remediate the contaminated soil. The changes in the concentrations of four main contaminants, including ENB, BP, MST, and PP, before and after remediation are listed in Table 1. The concentrations of ENB, BP, MST, and PP decreased from 1.564, 0.191, 0.315 and  $1.702 \text{ mg kg}^{-1}$  to 0.004, 0.002,  $<0.001$  and  $0.004 \text{ mg kg}^{-1}$ , respectively, with a depth of 0–20 cm after the remediation with PS activated by nZVI/BC after 360 days. The corresponding removal efficiency of these contaminants was 99.7%, 99.1%, 99.9% and 99.7%, respectively. The degradation of pollutants at different soil depths was also examined. In the topsoil (0–20 cm), the removal efficiency of these contaminants ranged from 99.1% to 99.9%, while the values were 98.5–99.8% in the soil with a depth of 20–40 cm. However, the degradation efficiency of these pollutants was slightly decreased in the deeper soil (40–80 cm). The removal efficiency was 88.6%, 98.5%, 99.2% and 99.6% for ENB, BP, MST and PP, respectively. These results suggest that the combination of nZVI/BC and PS would remediate these contaminants efficiently in the different depth of soil.



To further verify the role of PS activated by nZVI/BC in the degradation of pollutants, the control experiments such as ZVI or BC alone and their combination with PS were conducted (Additional file 1: Fig. S2). The degradation efficiency of contaminant in the soil at different depths without any treatment was 66.5–80.9%, 79.9–96.7%, 95.3–98.8%, and 95.9–98.9% for ENB, BP, MST and PP, respectively. The removal of these contaminants in CK mainly accounts for microbial degradation, including co-metabolism and catabolism (Kumar et al. 2018). The removal efficiency of ENB is relatively lower than other contaminants, probably owing to its higher toxicity (from its nitro group) to soil microorganisms (Yang et al. 2019). In addition, the application of PS could also lead to the removal of contaminants. The degradation efficiency of contaminants in the soil at different depths with PS was 74.0–88.8%, 84.8–97.5%, 94.6–98.2%, and 98.9–99.2% for ENB, BP, MST, and PP, respectively. The application of oxidants is generally thought to inhibit the microbial activity. Although PS might inhibit the microbial activity, PS can also be activated by soil components, such as soil minerals and organic matters, and generate free radicals for abiotic degradation of contaminants (Pathy et al. 2020). Furthermore, the addition of nZVI in PS slightly enhanced the removal of contaminants. The degradation efficiency of contaminants in the soil at different depths with nZVI and PS was 86.9–99.1%, 91.1–97.6%, 97.9–98.9%, and 97.3–99.2% for ENB, BP, MST, and PP, respectively. PS was activated by nZVI to generate  $\text{SO}_4^{\cdot-}$  and OH. The application of nZVI was supposed to improve the utilization efficiency of oxidants (Qiao et al. 2019), thus enhancing the degradation of pollutants. Moreover, the application of BC and PS also showed a relatively high efficiency in the removal of pollutants. The degradation efficiency in the soil at different

depths with BC and PS was 60.0–98.8%, 89.4–96.7%, 96.6–98.5%, and 98.2–99.6% for ENB, BP, MST, and PP, respectively. Biochar generally contains defects caused by structural collapse and produces persistent free radicals, which can activate PS to generate  $\text{SO}_4^{\cdot-}$  and OH for the degradation of pollutants (Hua et al. 2022). Lastly, the combination of nZVI/BC and PS showed the highest removal efficiency for different contaminants. The degradation efficiency in the soil at different depths with nZVI/BC and PS was 93.4–99.9%, 98.5–99.1%, 99.3–99.6%, and 99.5–99.7% for ENB, BP, MST, and PP, respectively. The support of biochar can protect nZVI from aggregation and oxidation in soil, which accordingly participated in the activation of PS more efficiently (Farooqi et al. 2020). Therefore, the combination of biochar and nZVI significantly enhanced the degradation efficiency of pollutants.

Although the natural attenuation of pollutants may play an important role in the annual remediation, chemical oxidation promotes faster degradation of contaminants in a shorter period. So, we further calculated the observed pseudo-first-order degradation rates of pollutants ( $k_{\text{obs}}$ ) to characterize these processes. As shown in Fig. 3, the degradation rate of ENB, BP, MST and PP in CK was  $(0.4\text{--}0.6) \times 10^{-2}$ ,  $(0.5\text{--}0.9) \times 10^{-2}$ ,  $(0.9\text{--}1.2) \times 10^{-2}$ , and  $(0.9\text{--}1.4) \times 10^{-2} \text{ d}^{-1}$ , respectively. The  $k_{\text{obs}}$  for PS was  $(0.4\text{--}0.6) \times 10^{-2}$ ,  $(0.7\text{--}1.0) \times 10^{-2}$ ,  $(0.9\text{--}1.2) \times 10^{-2}$ , and  $(1.3\text{--}1.4) \times 10^{-2} \text{ d}^{-1}$ , which was not significantly different from that of CK. The degradation rate of ENB, BP, MST and PP with BC/PS was  $(0.3\text{--}1.0) \times 10^{-2}$ ,  $(0.7\text{--}1.8) \times 10^{-2}$ ,  $(1.0\text{--}1.2) \times 10^{-2}$ , and  $(1.3\text{--}1.6) \times 10^{-2} \text{ d}^{-1}$ , respectively. Compared with CK, the  $k_{\text{obs}}$  of pollutant degradation was significant accelerated by BC/PS, which was attributed to the activation of PS by BC. It has been well established that biochar contains abundant oxygen-containing functional groups and can form persistent free radicals, which



are able to activate PS and degrade contaminants (Hu et al. 2020). The degradation rate of ENB, BP, MST, and PP with nZVI/PS was  $(0.3\text{--}1.1) \times 10^{-2}$ ,  $(0.8\text{--}1.1) \times 10^{-2}$ ,  $(1.1\text{--}1.3) \times 10^{-2}$ , and  $(1.1\text{--}1.4) \times 10^{-2} \text{ d}^{-1}$ , respectively, which was slightly higher than that of CK. Although nZVI exhibited excellent performance for PS activation in aqueous solutions, it had limited contribution to PS activation without the support of biochar in soil due to the tendency of aggregation and oxidation.

In contrast, the degradation rate of ENB, BP, MST and PP with nZVI/BC combined with PS was  $(0.7\text{--}1.8) \times 10^{-2}$ ,  $(1.2\text{--}1.3) \times 10^{-2}$ ,  $(1.5\text{--}1.6) \times 10^{-2}$ , and  $(1.6\text{--}1.8) \times 10^{-2} \text{ d}^{-1}$ , respectively, which was about 0.1–3.2 times higher than that of other treatments. This is due to the fact that nZVI can avoid aggregation and oxidation in soil with the support of biochar, and thus enhance PS activation for pollutant degradation. In addition, the further increase of nZVI/BC dosage to  $0.5 \text{ g kg}^{-1}$  could not significantly accelerate the rate of pollutant degradation. For example,  $k_{\text{obs}}$  of ENB, BP, MST and PP changed insignificantly at the soil depth of 0–40 cm, while their corresponding  $k_{\text{obs}}$  increased from  $0.7 \times 10^{-2}$  to  $0.8 \times 10^{-2}$ ,  $1.3 \times 10^{-2}$  to  $1.4 \times 10^{-2}$ ,  $1.5 \times 10^{-2}$  to  $1.6 \times 10^{-2}$ , and  $1.6 \times 10^{-2}$  to  $2.3 \times 10^{-2} \text{ d}^{-1}$ , respectively, at the soil depth of 40–80 cm. The probable reason was that the increase of nZVI/BC dosage resulted in the increase of nZVI/BC particles to the soil depth, which activated PS efficiently for pollutant degradation. These results indicate that the excessive nZVI/BC would compete with pollutant for the consumption of free radicals due to the quenching reactions between nZVI/BC and free radicals. Similar quenching reaction were also reported in nZVI/PS or mineral/PS in the previous studies (Liu et al. 2016, 2022; Zhu et al. 2016, 2018). Generally, the application of nZVI and BC both slightly accelerated the removal of contaminants, while the combination of them can significantly enhanced the degradation rates.

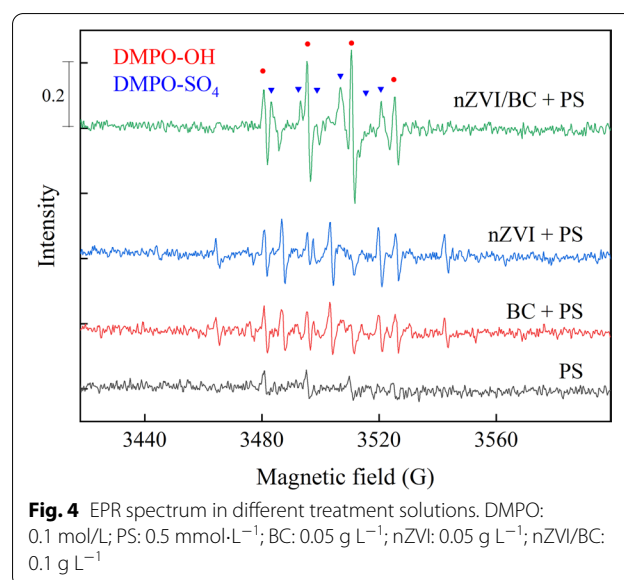
In addition, the depth of soil slightly influences the removal of contaminants. The difference in degradation rates at different depths in CK was mainly attributed to the microbial process. For example, the order of degradation rates of ENB was 0–20 cm ( $3.5 \times 10^{-3} \text{ d}^{-1}$ ) < 20–40 cm ( $5.6 \times 10^{-3} \text{ d}^{-1}$ ) < 40–80 cm ( $5.7 \times 10^{-3} \text{ d}^{-1}$ ), suggesting that ENB can be degraded faster in deep soil. According to the electron-deficient property of aromatic nitro groups, removal of ENB by oxidation reactions is typically difficult. Reduction of the nitro group in ENB is an altered method, usually executed by anaerobic strains, which tend to inhabit in the deeper soil (Wang et al. 2020). Therefore, the microbial degradation of ENB was faster in deep soil. On the contrary, the degradation of BP in topsoil ( $9.3 \times 10^{-3} \text{ d}^{-1}$ ) was significantly faster than that in deep soil ( $6.8 \times 10^{-3} \text{ d}^{-1}$ ). It has

been reported that BP is easily degraded under aerobic conditions, with the meta-ring cleavage product, which has been observed in most of the bacteria studied especially by the *Pseudomonas* sp. and *Micrococcus* sp. (Borja et al. 2005). So, the degradation rate of BP was higher than that in aerobic topsoil. Unlike in CK, the removal in treatments with nZVI/BC and PS mainly attributed to chemical oxidation. The degradation rate of contaminants at 0–20 cm ( $(1.3\text{--}1.8) \times 10^{-2} \text{ d}^{-1}$ ) showed no significant difference from that at 20–40 cm ( $(1.2\text{--}1.8) \times 10^{-2} \text{ d}^{-1}$ ), but slightly higher than that at 40–80 cm ( $(0.7\text{--}1.6) \times 10^{-2} \text{ d}^{-1}$ ). This probably was attributed to the large amounts of reductive organic matters in deep soil (Liang et al. 2021), which could consume free radicals from the activation of PS, and thus inhibit the decay of contaminants. It is noted that the inhibition was slight, and the degradation speed was still significantly faster than that of microbial degradation ( $(0.5\text{--}0.9) \times 10^{-2} \text{ d}^{-1}$  in CK).

In summary, the contaminants were dramatically removed after remediation with different treatments. Although the natural attenuation of pollutants by microorganisms plays an important role, the chemical oxidation promotes faster degradation of contaminants in a shorter period. The degradation rates of contaminants were significantly accelerated with addition of nZVI or BC with PS, compared with CK. The combination of nZVI/BC and PS could efficiently degrade contaminants at a considerably faster speed in both topsoil and deep soil.

### 3.3 Detection of reactive oxygen species

EPR coupled with DMPO as a spin-trapping agent was used to evaluate the capacity of ROS generation from



PS activation by nZVI/BC. As shown in Fig. 4, the typical pattern of hydroxyl radicals (OH) adducted to DMPO is a four-line spectrum with intensity ratio of 1:2:2:1 and hyperfine splitting constants of 14.89 G (Zeng et al. 2021). The typical six-line pattern of sulfate radical ( $\text{SO}_4^{\cdot-}$ ) adducted to DMPO is also observed (Song et al. 2019). ZVI would transfer electrons to persulfate, and generate sulfate radicals, sulfate ions, and ferrous ions, and ferrous ions also further transfer electrons to persulfate to yield  $\text{SO}_4^{\cdot-}$ .  $\text{SO}_4^{\cdot-}$  is inclined to produce OH by abstraction of electron from hydroxyl ion (Song et al. 2019).

For PS without addition, a relatively weaker signal of DMPO-OH was observed, attributed to the generation of OH from transformation of  $\text{SO}_4^{\cdot-}$ . The signal of DMPO- $\text{SO}_4$  was too weak to be detected probably due to the rapid shift from  $\text{SO}_4^{\cdot-}$  to OH (Eq. 6). Both DMPO- $\text{SO}_4$  and DMPO-OH could be detected in PS/nZVI or PS/BC, which was ascribed to the activation of PS by nZVI or BC which also produced  $\text{SO}_4^{\cdot-}$  and OH according to previous studies (Fang et al. 2014, 2015). With the activation of PS by nZVI/BC, the peak intensities of DMPO- $\text{SO}_4$  and DMPO-OH were significantly higher than those of PS activation by nZVI or BC alone, which suggested that more  $\text{SO}_4^{\cdot-}$  and OH were generated from PS activated by nZVI/BC. Consequently, the high efficiency of nZVI/BC in activation of PS exhibited a promising capacity for the degradation of contaminants during the remediation.

### 3.4 Changes of soil enzyme activity during the remediation

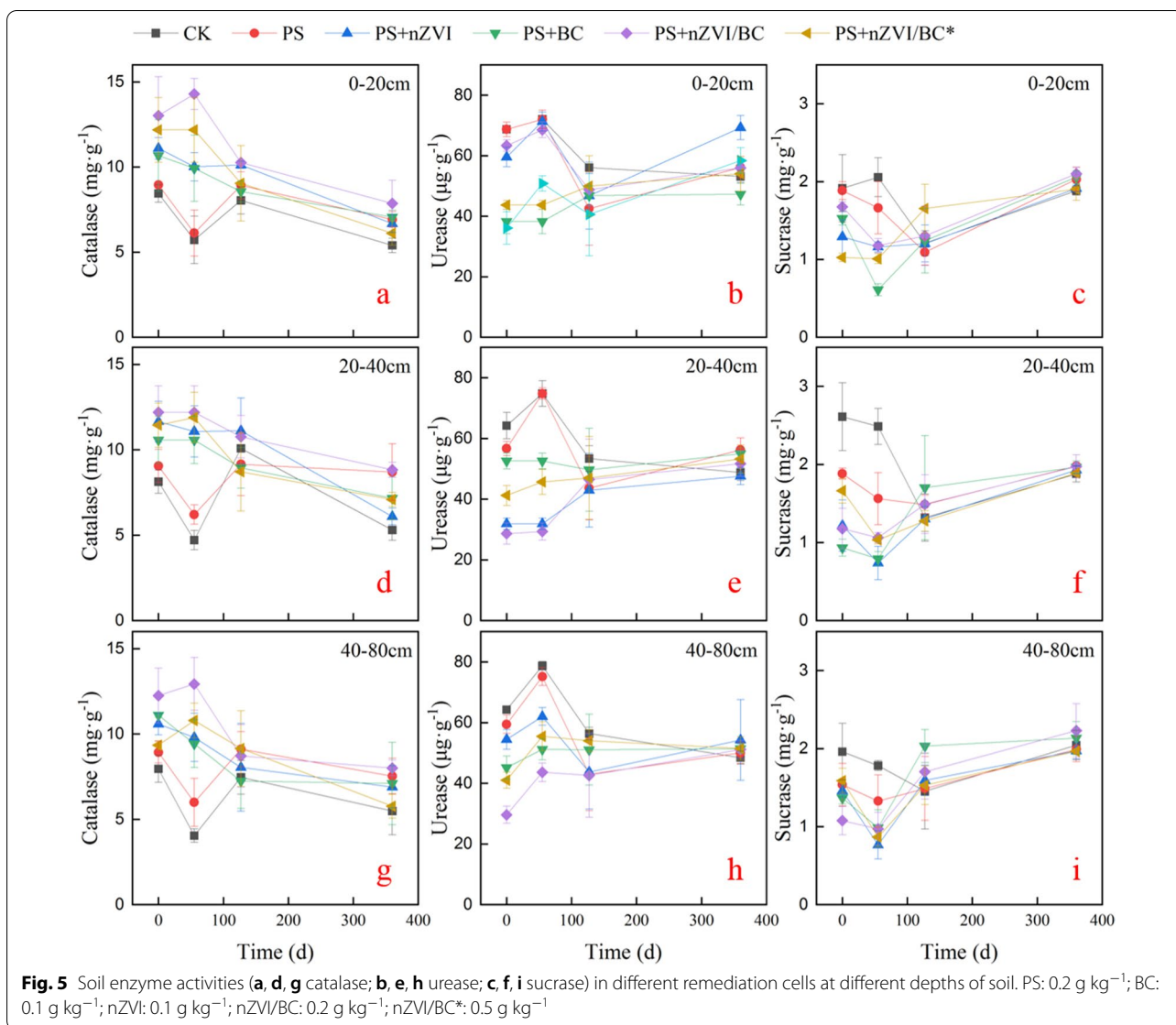
Despite the relatively low dosage of oxidant and material applied in this remediation, it might also change the soil environment to a certain extent. It has been reported that soil biological index is more sensitive to the change in soil environment compared with the physical and chemical properties of soil (Yao et al. 2006). Soil enzyme activities, showing quick responses to natural and anthropogenic disturbances (Song et al. 2019), were chosen as indicators to assess the ecological influence of remediation. As shown in Fig. 5, enzyme activities of CK changed slightly during the remediation, which was influenced by various factors, including soil temperature, moisture, and acidity (Baligar et al. 2008b). These were beyond the range of this study. To explore the effect of nZVI/BC and PS addition on soil enzyme activity, we compared the enzyme activities of different treatments.

Catalase is a signal for oxidative stress, which could prevent microorganisms from the attack of reactive free radicals (Cullen et al. 2011). As shown in Fig. 5, catalase activities of PS were slightly higher than those of CK at the depth of 20–80 cm, while showed an insignificant difference from those of CK at the depth of 0–20 cm. As

discussed above, PS could be activated by soil minerals to produce free radicals, which induce oxidative stresses on soil microorganisms to produce more catalase. Previous studies have proven both Fe(II) and Fe(III) would activate PS, but Fe(II) is the critical activator for PS to form sulfate radicals, which commonly appear in minerals in deeper soil, such as pyrite, magnetite, and siderite (Fang et al. 2018; Liu et al. 2016). To further test these processes, Both Fe and Mn contents in the different depth of soil were determined. As shown in Additional file 1: Table S2, the Fe and Mn content ranged from 16.69 to 18.79 and 0.101 to 0.108 g kg<sup>-1</sup>, respectively, whereas the deep soil contained more Fe. Furthermore, the content of Fe(II) in deep soil would be higher than that of top soil due to the anaerobic conditions as demonstrated in the previous studies (Abdelmoula et al. 1998; Wang et al. 2018). Therefore, stronger oxidative stresses were observed in deep soil, while insignificant in topsoil due to the lack of activators for PS. Upon application of materials (nZVI, BC, and nZVI/BC), the catalase activities were significantly enhanced, especially at the early stage (0–127 days) of remediation. On the 55th day, the catalase activities of nZVI-PS, BC-PS, nZVI/BC-PS and nZVI/BC-PS increased by 0.8–1.4 times, 0.7–1.3 times, 1.5–2.2 times, and 1.1–1.7 times, respectively, compared with those of CK. The nZVI and biochar both can activate PS to produce free radicals, which cause oxidative stress. The oxidative stress in nZVI/BC-PS was much greater, owing to the higher efficiency of free radical production by the combination of nZVI and BC. In addition, the order of increasing multiples in nZVI/BC treatments at different depths was 40–80 cm (2.2 and 1.7 times) > 20–40 cm (1.6 and 1.5 times) > 0–20 cm (1.5 and 1.1 times), suggesting that oxidative stress was heavier in deep soil. The microorganisms in deep soil inhabited in a more reductive environment, so they suffered stronger stress from the reactive oxygen species. They exhibited a more intense response and produced more catalase than those in topsoil. As the remediation progressed, the oxidative stress decreased gradually. As shown in Fig. 5, on the 360th day, the catalase activities of nZVI-PS, BC-PS, nZVI/BC-PS, and nZVI/BC-PS were only 0.2–0.7 times, 0.2–0.8 times, 0.4–1.0 times, and 0.1–0.5 times, higher than those of CK. The weakening of oxidative stress is attributed to the consumption of oxidants and inactivation of the material during the remediation.

Urease and sucrase participate in the transformation, decomposition, and mineralization of organic matter and nitrogen in the soil, which are closely related to microbial activities (Baligar et al. 2008a). As shown in Fig. 5, urease and sucrase activities of PS were slightly lower than those of CK at the early stage of remediation (before the 127th day). The decrease of urease and





sucrase activities was ascribed to the inhibition of microbial activities by free radicals, induced by activation of PS by soil minerals and organic matters. It is noted that the inhibition effect was insignificant in topsoil (0–20 cm), probably due to the relatively low content of Fe and Fe(II) contributed to PS activation producing less free radicals (Additional file 1: Table S2). Upon application of materials (nZVI, BC, and nZVI/BC), the urease and sucrase activities significantly decreased, especially at the early stage (before the 127th day) of remediation. Compared with CK, the urease activities of nZVI-PS, BC-PS, nZVI/BC-PS and nZVI/BC-PS decreased by 1–57%, 30–47%, 5–61%, and 30–39%, respectively, at the 55th day. The values for sucrase were 44–70%, 45–70%, 43–57%, and 51–58%. The application of materials and oxidants

generated amounts of free radicals, which have harmful effects on essential cellular macromolecules such as proteins, lipids, and nucleic acids (Staerck et al. 2017). Therefore, the chemical oxidation inhibited the microbial activities and thus decreased the urease and sucrase.

However, as the remediation progressed, the inhibition effect gradually declined, and disappeared at the end of remediation. As shown in Fig. 5, urease and sucrase activities of all treatments showed no significant difference with those of CK, suggesting that the microbial activity had recovered from chemical oxidation, attributed to the decline of oxidants in the soil. In addition, some sucrase activities after chemical oxidation remediation were slightly higher than those of CK. For example, the sucrase activity of nZVI/BC-PS (8.0 mg·g<sup>-1</sup>) was 45%

higher than that of CK ( $5.5 \text{ mg g}^{-1}$ ) at the 360th day. The probably reason for the promotion is that the chemical remediation removed pollutants more thoroughly, providing a more comfortable environment for microorganism growth. In addition, the reactive free radicals can also react with soil organic matters, and transfer macromolecular organic matters into low-molecular and available organic matters for microorganisms, promoting the sucrase activities for utilization of carbon source (Stubbins et al. 2010).

In summary, the application of materials and persulfate inhibits microbial activities and causes oxidative stress due to chemical oxidation at the early stage of remediation. Fortunately, this inhibition impact and oxidative stress disappeared at the later stage of remediation, which was ascribed to the depletion of oxidation. In addition, chemical oxidation also brought some positive impacts on soil microorganism activities after remediation.

#### 4 Conclusions

In this work, we yielded a biochar-supported nano-scale zerovalent iron (nZVI/BC) material by using the ball milling method in mass production. Subsequently, nZVI/BC was successfully applied in an in-situ pilot-scale soil remediation by activation of persulfate. All pollutants in soil were effectively degraded with degradation efficiency exceeding 99%, and the effects of nZVI/BC on soil enzyme activity were also evaluated. It was found that nZVI/BC-PS inhibited soil urease and sucrase enzyme activities at beginning of the injection (< 55 days), and these inhibition effects disappeared with remediation time prolonged (> 127 days). Our research provides a useful implementation case of remediation with nZVI/BC-PS activation and verifies its feasibility in practical contaminated soil remediation. However, other scientific issues such as nZVI/BC transport processes, kinetics of free radical evolution and potential risks of particles to groundwater would be considered in our future studies.

#### Supplementary Information

The online version contains supplementary material available at <https://doi.org/10.1007/s42773-022-00188-5>.

**Additional file 1. Text S1.** Chemicals. **Text S2.** EPR parameters. **Table S1.** Technical parameters of in-situ injection device. **Table S2.** Total Fe and Mn concentration of soil in different depths. **Figure S1.** The in-situ injection device for nanomaterials. **Figure S2.** Concentrations of contaminants in soil with different treatments.

#### Acknowledgements

Not applicable.

#### Author contributions

YZ: formal analysis, writing—original draft, and writing—review and editing. TL: methodology and writing—original draft. YD: investigation and methodology. GF: formal analysis, writing—review and editing, project administration,

funding acquisition, and supervision. XW: investigation. BY: investigation. LG: funding acquisition. JG: writing—review and editing. YW: writing—review and editing. DZ: writing—review and editing. All authors read and approved the final manuscript.

#### Funding

This work was supported by grants from the National Key Research and Development Program of China (2018YFC1802006, 2017YFA0207001), the National Natural Science Foundation of China (42022049, 42130707, and 42107045), and the 145 Program of Institute of Soil Science (ISSASIP2213).

#### Availability of data and materials

Data can be found in supplementary material. Supplementary material associated with this article can be found, in the online version.

#### Declarations

##### Competing interests

The authors declare no competing financial interest.

##### Author details

<sup>1</sup>Key Laboratory of Soil Environment and Pollution Remediation, Institute of Soil Science, Chinese Academy of Sciences, Nanjing 210008, People's Republic of China. <sup>2</sup>University of Chinese Academy of Sciences, Beijing 100049, People's Republic of China. <sup>3</sup>School of Environmental and Safety Engineering, Changzhou University, Changzhou 213164, China. <sup>4</sup>School of Earth and Environment, Anhui University of Science and Technology, Huainan 232001, People's Republic of China. <sup>5</sup>Geological Survey of Jiangsu Province, Nanjing 210018, People's Republic of China. <sup>6</sup>State Key Laboratory of Pollution Control and Resource Reuse, School of the Environment, Nanjing University, Nanjing 210023, People's Republic of China.

Received: 8 September 2022 Revised: 6 November 2022 Accepted: 8 November 2022

Published online: 05 December 2022

#### References

- Abdelmoula M, Trolard F, Bourrié G, Génin JMR (1998) Evidence for the Fe(II)-Fe(III) Green Rust "Fougerite" mineral occurrence in a hydromorphic soil and its transformation with depth. *Hyperfine Interact* 112(1):235–238. <https://doi.org/10.1023/A:1010802508927>
- Baligar VC, Staley TE, Wright RJ (2008a) Enzyme activities in appalachian soils: 2. Urease. *Commun Soil Sci Plant Anal* 22(3–4):315–322. <https://doi.org/10.1080/00103629109368418>
- Baligar VC, Wright RJ, Fageria NK, Pitta GVE (2008b) Enzyme activities in Cerado soils of Brazil. *Commun Soil Sci Plant Anal* 30(9–10):1551–1560. <https://doi.org/10.1080/00103629909370306>
- Borja J, Taleon DM, Auresenia J, Gallardo S (2005) Polychlorinated biphenyls and their biodegradation. *Process Biochem* 40(6):1999–2013. <https://doi.org/10.1016/j.procbio.2004.08.006>
- Cullen LG, Tilston EL, Mitchell GR, Collins CD, Shaw LJ (2011) Assessing the impact of nano- and micro-scale zerovalent iron particles on soil microbial activities: particle reactivity interferes with assay conditions and interpretation of genuine microbial effects. *Chemosphere* 82(11):1675–1682. <https://doi.org/10.1016/j.chemosphere.2010.11.009>
- Delgado F, Gutierrez VS, Dennehy M, Alvarez M (2020) Stable and efficient metal-biochar supported catalyst: degradation of model pollutants through sulfate radical-based advanced oxidation processes. *Biochar* 2(3):319–328. <https://doi.org/10.1007/s42773-020-00058-y>
- Dionysiou DD, Balasubramanian G, Suidan MT, Khodadoust AP, Baudin I, Laine J-M (2000) Rotating disk photocatalytic reactor: development, characterization, and evaluation for the destruction of organic pollutants in water. *Water Res* 34(11):2927–2940. [https://doi.org/10.1016/S0043-1354\(00\)00022-1](https://doi.org/10.1016/S0043-1354(00)00022-1)
- Dong H, He Q, Zeng G, Tang L, Zhang L, Xie Y, Zeng Y, Zhao F (2017) Degradation of trichloroethene by nanoscale zero-valent iron (nZVI) and nZVI activated persulfate in the absence and presence of EDTA. *Chem Eng J* 316:410–418. <https://doi.org/10.1016/j.cej.2017.01.118>

- Fang G, Gao J, Liu C, Dionysiou DD, Wang Y, Zhou D (2014) Key role of persistent free radicals in hydrogen peroxide activation by biochar: implications to organic contaminant degradation. *Environ Sci Technol* 48(3):1902–1910. <https://doi.org/10.1021/es4048126>
- Fang G, Liu C, Gao J, Dionysiou DD, Zhou D (2015) Manipulation of persistent free radicals in biochar to activate persulfate for contaminant degradation. *Environ Sci Technol* 49(9):5645–5653. <https://doi.org/10.1021/es5061512>
- Fang G, Chen X, Wu W, Liu C, Dionysiou DD, Fan T, Wang Y, Zhu C, Zhou D (2018) Mechanisms of interaction between persulfate and soil constituents: activation, free radical formation, conversion, and identification. *Environ Sci Technol* 52(24):14352–14361. <https://doi.org/10.1021/acs.est.8b04766>
- Farooqi ZH, Begum R, Naseem K, Wu W, Irfan A (2020) Zero valent iron nanoparticles as sustainable nanocatalysts for reduction reactions. *Catalysis Reviews*. <https://doi.org/10.1080/01614940.2020.1807797>
- Guo J, Wen X, Yang J, Fan T (2020) Removal of benzo(a)pyrene in polluted aqueous solution and soil using persulfate activated by corn straw biochar. *J Environ Manage* 272:111058. <https://doi.org/10.1016/j.jenvm.2020.111058>
- Hazime R, Nguyen QH, Ferronato C, Salvador A, Jaber F, Chovelon JM (2014) Comparative study of imazalil degradation in three systems: UV/TiO<sub>2</sub>, UV/K<sub>2</sub>S<sub>2</sub>O<sub>8</sub> and UV/TiO<sub>2</sub>/K<sub>2</sub>S<sub>2</sub>O<sub>8</sub>. *Appl Catal B* 144:286–291. <https://doi.org/10.1016/j.apcatb.2013.07.001>
- Hu B, Ai Y, Jin J, Hayat T, Alsaedi A, Zhuang L, Wang X (2020) Efficient elimination of organic and inorganic pollutants by biochar and biochar-based materials. *Biochar* 2(1):47–64. <https://doi.org/10.1007/s42773-020-00044-4>
- Hua L, Cheng T, Liang Z, Wei T (2022) Investigation of the mechanism of phytate-modified biochar-catalyzed persulfate degradation of Ponceau 2R. *Biochar*. <https://doi.org/10.1007/s42773-022-00136-3>
- Huang M, Wang X, Liu C, Fang G, Gao J, Wang Y, Zhou D (2021) Facile ball milling preparation of sulfur-doped carbon as peroxydisulfate activator for efficient removal of organic pollutants. *J Environ Chem Eng*. <https://doi.org/10.1016/j.jece.2021.106536>
- Kumar S, Kaushik G, Dar MA, Nimesh S, López-Chuken, U.J. and Villarreal-Chiu, J.F. (2018) Microbial degradation of organophosphate pesticides: a Review. *Pedosphere* 28(2):190–208. [https://doi.org/10.1016/s1002-0160\(18\)60017-7](https://doi.org/10.1016/s1002-0160(18)60017-7)
- Li H, Zhu F, He S (2019) The degradation of decabromodiphenyl ether in the e-waste site by biochar supported nanoscale zero-valent iron/persulfate. *Ecotoxicol Environ Saf* 183:109540. <https://doi.org/10.1016/j.ecoenv.2019.109540>
- Liang L, Xi F, Tan W, Meng X, Hu B, Wang X (2021) Review of organic and inorganic pollutants removal by biochar and biochar-based composites. *Biochar* 3(3):255–281. <https://doi.org/10.1007/s42773-021-00101-6>
- Liu H, Bruton TA, Li W, Buren JV, Prasse C, Doyle FM, Sedlak DL (2016) Oxidation of benzene by persulfate in the presence of Fe(III)- and Mn(IV)-containing oxides: stoichiometric efficiency and transformation products. *Environ Sci Technol* 50(2):890–898. <https://doi.org/10.1021/acs.est.5b04815>
- Liu J, Jiang S, Chen D, Dai G, Wei D, Shu Y (2020) Activation of persulfate with biochar for degradation of bisphenol A in soil. *Chem Eng J*. <https://doi.org/10.1016/j.cej.2019.122637>
- Liu T, Yao B, Luo Z, Li W, Li C, Ye Z, Gong X, Yang J, Zhou Y (2022) Applications and influencing factors of the biochar-persulfate based advanced oxidation processes for the remediation of groundwater and soil contaminated with organic compounds. *Sci Total Environ*. <https://doi.org/10.1016/j.scitotenv.2022.155421>
- Lu L, Yu W, Wang Y, Zhang K, Zhu X, Zhang Y, Wu Y, Ullah H, Xiao X, Chen B (2020) Application of biochar-based materials in environmental remediation: from multi-level structures to specific devices. *Biochar* 2(1):1–31. <https://doi.org/10.1007/s42773-020-00041-7>
- Ouyang D, Yan J, Qian L, Chen Y, Han L, Su A, Zhang W, Ni H, Chen M (2017) Degradation of 1,4-dioxane by biochar supported nano magnetite particles activating persulfate. *Chemosphere* 184:609–617. <https://doi.org/10.1016/j.chemosphere.2017.05.156>
- Pathy A, Ray J, Paramasivan B (2020) Biochar amendments and its impact on soil biota for sustainable agriculture. *Biochar* 2(3):287–305. <https://doi.org/10.1007/s42773-020-00063-1>
- Pignatello JJ, Oliveros E, MacKay A (2006) Advanced oxidation processes for organic contaminant destruction based on the fenton reaction and related chemistry. *Crit Rev Environ Sci Technol* 36(1):1–84. <https://doi.org/10.1080/10643380500326564>
- Qiao J, Yu H, Wang X, Li F, Wang Q, Yuan Y, Liu C (2019) The applicability of biochar and zero-valent iron for the mitigation of arsenic and cadmium contamination in an alkaline paddy soil. *Biochar* 1(2):203–212. <https://doi.org/10.1007/s42773-019-00015-4>
- Qiu M, Liu L, Ling Q, Cai Y, Yu S, Wang S, Fu D, Hu B, Wang X (2022) Biochar for the removal of contaminants from soil and water: a review. *Biochar*. <https://doi.org/10.1007/s42773-022-00146-1>
- Shaheen SM, Mosa A, Abdelrahman H, Niazi NK, Antoniadis V, Shahid M, Song H, Kwon EE, Rinklebe J (2022) Removal of toxic elements from aqueous environments using nano zero-valent iron- and iron oxide-modified biochar: a review. *Biochar*. <https://doi.org/10.1007/s42773-022-00149-y>
- Song Y, Fang G, Zhu C, Zhu F, Wu S, Chen N, Wu T, Wang Y, Gao J, Zhou D (2019) Zero-valent iron activated persulfate remediation of polycyclic aromatic hydrocarbon-contaminated soils: An in situ pilot-scale study. *Chem Eng J* 355:65–75. <https://doi.org/10.1016/j.cej.2018.08.126>
- Staerck C, Gastebois A, Vandeputte P, Calenda A, Larcher G, Gillmann L, Papon N, Bouchara JP, Fleury MJJ (2017) Microbial antioxidant defense enzymes. *Microb Pathog* 110:56–65. <https://doi.org/10.1016/j.micpath.2017.06.015>
- Stubbins A, Spencer RGM, Chen H, Hatcher PG, Mopper K, Hernes PJ, Mwamba VL, Mangangu AM, Wabakanghanzi JN, Six J (2010) Illuminated darkness: molecular signatures of Congo River dissolved organic matter and its photochemical alteration as revealed by ultrahigh precision mass spectrometry. *Limnol Oceanogr* 55(4):1467–1477. <https://doi.org/10.4319/lo.2010.55.4.1467>
- Sun Z, Feng L, Fang G, Chu L, Zhou D, Gao J (2021) Nano Fe<sub>3</sub>O<sub>4</sub> embedded in montmorillonite with citric acid enhanced photocatalytic activity of nanoparticles towards diethyl phthalate. *J Environ Sci (china)* 101:248–259. <https://doi.org/10.1016/j.jes.2020.08.019>
- Wang S, Ang HM, Tade MO (2008) Novel applications of red mud as coagulant, adsorbent and catalyst for environmentally benign processes. *Chemosphere* 72(11):1621–1635. <https://doi.org/10.1016/j.chemosphere.2008.05.013>
- Wang X, Sun L, Zhang Y, Xu X, Guo D, Shi Z (2018) Characterization of reduction of iron oxide and oxidation of ferrous iron in upland cinnamon soil profiles in West Henan, China. *Acta Pedol Sin* 55(5):1199–1211. <https://doi.org/10.11766/trxb201712070430>
- Wang H, Zhao HP, Zhu L (2020) Structures of nitroaromatic compounds induce Shewanella oneidensis MR-1 to adopt different electron transport pathways to reduce the contaminants. *J Hazard Mater* 384:121495. <https://doi.org/10.1016/j.jhazmat.2019.121495>
- Wu S, He H, Li X, Yang C, Zeng G, Wu B, He S, Lu L (2018) Insights into atrazine degradation by persulfate activation using composite of nanoscale zero-valent iron and graphene: Performances and mechanisms. *Chem Eng J* 341:126–136. <https://doi.org/10.1016/j.cej.2018.01.136>
- Wu P, Ata-Ul-Karim ST, Singh BP, Wang H, Wu T, Liu C, Fang G, Zhou D, Wang Y, Chen W (2019a) A scientometric review of biochar research in the past 20 years (1998–2018). *Biochar* 1(1):23–43. <https://doi.org/10.1007/s42773-019-00002-9>
- Wu Y, Chen X, Han Y, Yue D, Cao X, Zhao Y, Qian X (2019b) Highly efficient utilization of nano-Fe(0) embedded in mesoporous carbon for activation of peroxydisulfate. *Environ Sci Technol* 53(15):9081–9090. <https://doi.org/10.1021/acs.est.9b02170>
- Wu P, Wang Z, Wang H, Bolan NS, Wang Y, Chen W (2020) Visualizing the emerging trends of biochar research and applications in 2019: a scientometric analysis and review. *Biochar* 2(2):135–150. <https://doi.org/10.1007/s42773-020-00055-1>
- Wu P, Wang Z, Bolan NS, Wang H, Wang Y, Chen W (2021) Visualizing the development trend and research frontiers of biochar in 2020: a scientometric perspective. *Biochar* 3(4):419–436. <https://doi.org/10.1007/s42773-021-00120-3>
- Yan J, Han L, Gao W, Xue S, Chen M (2015) Biochar supported nanoscale zerovalent iron composite used as persulfate activator for removing trichloroethylene. *Biores Technol* 175:269–274. <https://doi.org/10.1016/j.biortech.2014.10.103>
- Yang P, Ji Y, Lu J, Huang Q (2019) Formation of nitrophenolic byproducts during heat-activated peroxydisulfate oxidation in the presence of natural organic matter and nitrite. *Environ Sci Technol* 53(8):4255–4264. <https://doi.org/10.1021/acs.est.8b06967>

- Yang B, Dai J, Zhao Y, Wu J, Ji C, Zhang Y (2022) Advances in preparation, application in contaminant removal, and environmental risks of biochar-based catalysts: a review. *Biochar*. <https://doi.org/10.1007/s42773-022-00169-8>
- Yao X-H, Min H, Lü Z-H, Yuan H-P (2006) Influence of acetamiprid on soil enzymatic activities and respiration. *Eur J Soil Biol* 42(2):120–126. <https://doi.org/10.1016/j.ejsobi.2005.12.001>
- Yao Y, Cai Y, Lu F, Wei F, Wang X, Wang S (2014) Magnetic recoverable  $\text{MnFe}_2\text{O}_4$  and  $\text{MnFe}_2\text{O}_4$ -graphene hybrid as heterogeneous catalysts of peroxy-monosulfate activation for efficient degradation of aqueous organic pollutants. *J Hazard Mater* 270:61–70. <https://doi.org/10.1016/j.jhazmat.2014.01.027>
- Yao B, Chen X, Zhou K, Luo Z, Li P, Yang Z, Zhou Y (2022) p-Arsanilic acid decontamination over a wide pH range using biochar-supported manganese ferrite material as an effective persulfate catalyst: Performances and mechanisms. *Biochar*. <https://doi.org/10.1007/s42773-022-00158-x>
- Zeng Y, Fang G, Fu Q, Dionysiou DD, Wang X, Gao J, Zhou D, Wang Y (2021) Photochemical characterization of paddy water during rice cultivation: formation of reactive intermediates for As(III) oxidation. *Water Res* 206:117721. <https://doi.org/10.1016/j.watres.2021.117721>
- Zeng Y, Fang G, Fu Q, Peng F, Wang X, Dionysiou DD, Guo J, Gao J, Zhou D, Wang Y (2022) Mechanistic study of the effects of agricultural amendments on photochemical processes in paddy water during rice growth. *Environ Sci Technol* 56(7):4221–4230. <https://doi.org/10.1021/acs.est.2c00145>
- Zhu C, Fang G, Dionysiou DD, Liu C, Gao J, Qin W, Zhou D (2016) Efficient transformation of DDTs with persulfate activation by zero-valent iron nanoparticles: a mechanistic study. *J Hazard Mater* 316:232–241. <https://doi.org/10.1016/j.jhazmat.2016.05.040>
- Zhu C, Zhu F, Dionysiou DD, Zhou D, Fang G, Gao J (2018) Contribution of alcohol radicals to contaminant degradation in quenching studies of persulfate activation process. *Water Res* 139:66–73. <https://doi.org/10.1016/j.watres.2018.03.069>

Submit your manuscript to a SpringerOpen<sup>®</sup> journal and benefit from:

- Convenient online submission
- Rigorous peer review
- Open access: articles freely available online
- High visibility within the field
- Retaining the copyright to your article

---

Submit your next manuscript at ► [springeropen.com](https://www.springeropen.com)

---